Supplemental Materials

Molecular Biology of the Cell

Liu et al.

Roles of the novel coiled-coil protein Rng10 in septum formation during fission yeast cytokinesis

Yajun Liu, I-Ju Lee, Mingzhai Sun, Casey A. Lower, Kurt W. Runge, Jianjie Ma, and Jian-Qiu Wu

Supplemental materials

Video Legend

Video 1: Cell lysis caused by *rng10*Δ at 25°C. The interval is 2 min in time-lapse confocal microscopy (UltraVIEW Vox CSUX1; PerkinElmer). DIC images are shown. Left, no lysis; middle, one daughter cell lysed; right, both daughter cells lysed. This video corresponds to Figure 1C. Display rate: 2 frames per second (fps).

Video 2: Localization and timing of Rng10-mEGFP (green) with a cell cycle marker SPB protein Sad1-tdTomato (red). The interval is 4 min in time-lapse confocal microscopy (UltraVIEW Vox CSUX1; PerkinElmer). DIC is shown on the left. The maximum intensity projections of the fluorescence images from 11 slices spaced at 0.6 μm at each time point are shown on the right. This video relates to Figure 2C. Display rate: 6 fps.

Video 3: Colocalization of Rng10-mEGFP (green) and Rga7-tdTomato (red). The interval is 2 s in time-lapse confocal microscopy (UltraVIEW Vox CSUX1; PerkinElmer). Two cells imaged at a single focal plane for mEGFP (left), tdTomato (middle), and merged (right) channels are shown. This video corresponds to Figure 4C. Display rate: 6 fps.

Supplemental Table 1: ***S. pombe*** **strains used in this study**

Strain name	Genotype	Figure/video/table/reference
JW81	*h⁻ ade6-210 ura4-D18 leu1-32*	Figs. 1 (A, B, and D-F), 4B, and 6A
JW5670	*h⁻ rng10Δ::kanMX6 ade6-210 ura4-D18 leu1-32*	Figs. 1 (A-F), 3F, and 6C; Table 2; and Video 1
JW5899	*rng10-mEGFP-kanMX6 rlc1-tdTomato-natMX6 ade6-M210 leu1-32 ura4-D18*	Fig. 2, A and B
JW6067	*rng10-mEGFP-kanMX6 sad1-tdTomato-natMX6 ade6 leu1-32 ura4-D18*	Fig. 2C and Video 2
JW949	*h⁻ rlc1-mYFP-kanMX6 ade6-M210 leu1-32 ura4-D18*	Fig. 2D
JW1092	*h⁻ spn1-mYFP-kanMX6 ade6-M210 leu1-32 ura4-D18*	Fig. 2D
JW5669	*h⁻ rng10-mECitrine-kanMX6 ade6-210 ura4-D18 leu1-32*	Figs. 2D, 3 (C-F), 4F, S2E, S4A; and Table 1
JW6075	*h⁻ spn1-mEOS3.2-kanMX6 ade6-210 leu1-32 ura4-D18*	Fig. 2D
JW6084	*h⁻ rng10-mEOS3.2-kanMX6 ade6-210 leu1-32 ura4-D18*	Fig. 2D
JW6085	*h⁻ rlc1-mEOS3.2-kanMX6 ade6-210 leu1-32 ura4-D18*	Fig. 2D
JW6658	*h⁻ rng10-mMaple3-kanMX6 ade6-210 leu1-32 ura4-D18*	Fig. 2D
JW6186	*h⁻ rng10(1-200)-mEGFP-kanMX6 ade6-M210 leu1-32 ura4-D18*	Figs. 3 (C-F) and S3A; and Table 1
JW6187	*h⁻ rng10(1-450)-mEGFP-kanMX6 ade6-M210 leu1-32 ura4-D18*	Figs. 3 (C-F) and S3A; and Table 1
JW6188	*h⁻ rng10(1-750)-mEGFP-kanMX6 ade6-M210 leu1-32 ura4-D18*	Figs. 3 (C-F) and S3A; and Table 1
JW6868	*Prng10-mECitrine-rng10(201-1038) ade6-M210 leu1-32 ura4-D18*	Figs. 3 (C-F) and S3A; and Table 1
JW6869	*Prng10-mECitrine-rng10(451-1038) ade6-M210 leu1-32 ura4-D18*	Figs. 3 (C-F) and S3A; and Table 1
JW7177	*Prng10-mECitrine-rng10(201-750)-5FLAG-kanMX6 ade6-M210 leu1-32 ura4-D18*	Figs. 3 (C, D, and F) and S3A; and Table 1
JW7195	*Prng10-mECitrine-rng10(751-1038) ade6-M210 leu1-32 ura4-D18*	Figs. 3 (C-F) and S3A; and Table 1
JW5016	*h⁻ leu1-32-kanMX6-P41nmt1-S_{Taq} ade6-M210 ura4-D18*	Fig. 4A
JW6023	*h⁻ rng10-S_{Taq}-kanMX6 ade6-M210 leu1-32 ura4-D18*	Fig. 4A
JW3661	*h⁻ rga7-mECitrine-kanMX6 ade6-210 leu1-32 ura4-D18*	Figs. 4 (B, D, G, and H), and S4A
JW6058	*h⁺ rng10-13Myc-hphMX6 ade6-210 leu1-32 ura4-D18*	Fig. 4B
JW6122	*rng10-13Myc-hphMX6 rga7-mECitrine-kanMX6 ade6-210 leu1-32 ura4-D18*	Fig. 4B
JW5943	*h⁻ rng10-mEGFP-kanMX6 rga7-tdTomato-natMX6 ade6 leu1-32 ura4-D18*	Fig. 4C and Video 3
JW4028	*h⁻ rga7Δ::kanMX6 ade6-M210 leu1-32 ura4-D18*	Figs. 4E, 6B, and S4F; and Table 2
JW6003	*rga7Δ::kanMX6 rng10-mECitrine-kanMX6 ade6 leu1-32 ura4-D18*	Figs. 4F
JW6044	*rng10Δ::kanMX6 rga7-mECitrine-kanMX6 ade6-210 leu1-32 ura4-D18*	Figs. 4, G and H
JW6988	*cdc7-GBP-hphMX6 rng10-mEGFP-kanMX6 rga7-tdTomato-natMX6 ade6 leu1-32 ura4-D18*	Fig. 4I
3166	*h⁻ ags1Δ 3'UTR$_{ags1}$⁺::ags1⁺-GFP:leu1⁺:ura4⁺ade6-M210 his3-D1 leu1-32 ura4-D18*	Fig. 5, A-C; Cortes *et al.*, 2012
JW6832	*rng10Δ::kanMX6 ags1Δ 3'UTR$_{ags1}$⁺::ags1⁺-GFP:leu1⁺:ura4⁺ade6-M210 his3-D1 leu1-32 ura4-D18*	Fig. 5, A-C
JW6833	*rga7Δ::natMX6 ags1Δ 3'UTR$_{ags1}$⁺::ags1⁺-GFP:leu1⁺:ura4⁺ade6 his3-D1 leu1-32 ura4-D18*	Fig. 5, A-C
JW5249	*GFP-bgs1-leu1⁺ bgs1Δ::ura4⁺ rlc1-tdTomato-natMX6 ade6-M210 leu1-32 ura4-D18*	Fig. 5, D-F
JW6108	*GFP-bgs1-leu1⁺ bgs1Δ::ura4⁺ rlc1-tdTomato-natMX6 rng10Δ::kanMX6 ade6-210 leu1-32 ura4-D18*	Fig. 5, D-F
JW6506	*GFP-bgs1-leu1⁺ bgs1Δ::ura4⁺ rlc1-tdTomato-natMX6 rga7Δ::kanMX6 ade6-M210 leu1-32 ura4-D18*	Fig. 5, D-F
562	*h⁺ bgs4Δ::ura4⁺ Pbgs4⁺::GFP-bgs4⁺-leu1⁺ leu1-32 ura4-D18 his3-D1*	Fig. 5, G-I; Cortes *et al.*, 2005

JW6752	*rng10Δ::kanMX6 bgs4Δ::ura4$^+$ Pbgs4$^+$::GFP-bgs4$^+$-leu1$^+$ ura4-D18 his3-D1*	Fig. 5, G-I
JW7043	*rga7Δ::kanMX6 bgs4Δ::ura4$^+$ Pbgs4$^+$::GFP-bgs4$^+$-leu1$^+$ ade6-M210? leu1-32 ura4-D18*	Fig. 5, G-I
JW2178	*h$^+$ rlc1-tdTomato-natMX6 sad1-mEGFP-kanMX6 ade6-M210 ura4-D18 leu1-32*	Fig. S1, A, D, and E
JW5677	*rng10Δ::kanMX6 rlc1-tdTomato-natMX6 sad1-mEGFP-kanMX6 ade6-210 ura4-D18 leu1-32*	Fig. S1, B, D, and E
JW6050	*rga7Δ::kanMX6 rlc1-tdTomato-natMX6 sad1-mEGFP-kanMX6 ade6-M210 leu1-32 ura4-D18*	Fig. S1, C, D, and E
JW3313	*h$^-$ leu1-32-kanMX6-3nmt1-mEGFP rlc1-tdTomato-natMX6 ade6-M210 ura4-D18*	Fig. S2, A and D
JW6160	*rng10Δ::kanMX6 leu1-32-kanMX6-3nmt1-mEGFP rlc1-tdTomato-natMX6 ade6-210 ura4-D18*	Fig. S2, B and D
JW6572	*rga7Δ::natMX6 leu1-32-kanMX6-3nmt1-mEGFP rlc1-tdTomato-natMX6 ade6-M210 ura4-D18*	Fig. S2, C and D
JW5675	*h$^-$ rng10-mEGFP-kanMX6 ade6-M210 leu1-32 ura4-D18*	Fig. S3, A-C; and Table 1
JW948	*h$^-$ rlc1-mEGFP-kanMX6 ade6-M210 leu1-32 ura4-D18*	Fig. S3, A and C; and Table 1
JW1091	*h- spn1-mEGFP-kanMX6 ade6-M210 leu1-32 ura4-D18*	Fig. S3, A and C; and Table 1
JW976	*h$^+$ cdc15-mEGFP-kanMX6 ade6-M210 leu1-32 ura4-D18*	Fig. S3, A and C; and Table 1
JW1109	*h$^+$ kanMX6-Pmyo2-mEGFP-myo2 ade6-M210 leu1-32 ura4-D18*	Fig. S3, A and C; and Table 1
JW6651	*rga7-mECitrine-kanMX6 rho2Δ::hphMX6 rng10Δ::kanMX6 ade6-210 leu1-32 ura4-D18*	Fig. S4B
JW6652	*rga7-mECitrine-kanMX6 rho2Δ::hphMX6 ade6-210 leu1-32 ura4-D18*	Fig. S4B
JW6962	*h$^-$ rga2-mECitrine-kanMX6 ade6-210 leu1-32 ura4-D18*	Fig. S4C
JW7034	*rng10Δ::hphMX6 rga2-mECitrine-kanMX6 ade6-210 leu1-32 ura4-D18*	Fig. S4C
JW6944	*h$^-$ rga8-mECitrine-kanMX6 ade6-210 ura4-D18 leu1-32*	Fig. S4D
JW7007	*rng10Δ::hphMX6 rga8-mECitrine-kanMX6 ade6-210 ura4-D18 leu1-32*	Fig. S4D
JW6989	*cdc7-GBP-hphMX6 rga7-tdTomato-natMX6 ade6 leu1-32 ura4-D18*	Fig. S4E
JW6990	*cdc7-GBP-hphMX6 rng10-mEGFP-kanMX6 ade6 leu1-32 ura4-D18*	Fig. S4E
JW6132	*h$^+$ rng10Δ::hphMX6 ade6-210 leu1-32 ura4-D18*	Fig. S4F and Table 2
JW6295	*h$^-$ rng10Δ::kanMX6 ade6-210 leu1-32 ura4-D18* + pUR19	Fig. S5A
JW6163	*h$^-$ rng10Δ::kanMX6 ade6-210 leu1-32 ura4-D18* + pUR19-Rho1	Fig. S5A
JW6306	*h$^-$ rga7Δ::kanMX6 ade6-M210 leu1-32 ura4-D18* + pUR19	Fig. S5A
JW6164	*h$^-$ rga7Δ::kanMX6 ade6-M210 leu1-32 ura4-D18* + pUR19-Rho1	Fig. S5A
JW6548	*h$^+$ GFP-syb1-kanMX6 rlc1-tdTomato-natMX6 ade6 leu1-32 ura4-D18*	Fig. S5B
JW7088	*rng10Δ::hphMX6 GFP-syb1-kanMX6 rlc1-tdTomato-natMX6 ade6 leu1-32 ura4-D18*	Fig. S5B
JW7092	*rga7Δ::natMX6 GFP-syb1-kanMX6 rlc1-tdTomato-natMX6 ade6 leu1-32 ura4-D18*	Fig. S5B
MBY887	*h$^+$ sec8-1 leu1-32 ura4-D18*	Fig. S5C; Wang *et al.*, 2002
PPG6840	*h$^-$ rho1-596-natMX6 leu1-32 ura4D-18*	Table 2; Viana *et al.*, 2013
JW289	*h$^+$ spn1-Δ2::kanMX6 leu1-32 ura4-D18*	Table 2
JW713	*h$^+$ myp2-Δ2::kanMX6 ade6-M210 leu1-32 ura4-D18*	Table 2
JW1374	*h$^-$ cdc7-24 ade6-M210 leu1-32 ura4-D18*	Table 2
JW1636	*h$^+$ mid1-6 ade6-M210 leu1-32 ura4-D18*	Table 2
JW1696	*h$^+$ bgs1-191 ade6-M210 leu1-32 ura4-D18*	Table 2
JW2543	*h$^-$ art1Δ::ura4$^+$ ade6-M216 leu1-32 ura4-D18*	Table 2
JW2640	*h$^+$ pxlΔ::kanMX4 ade6 leu1-32 ura4-D18*	Table 2; Kim *et al.*, 2010

JW2716	*h$^+$ exo70Δ::kanMX4 ade6 leu1-32 ura4-D18*	Table 2; Kim *et al.*, 2010
JW2719	*h$^+$ rga8Δ::kanMX4 ade6 leu1-32 ura4-D18*	Table 2; Kim *et al.*, 2010
JW3962	*h$^+$ rho2Δ::kanMX4 ade6 leu1-32 ura4-D18*	Table 2; Kim *et al.*, 2010
YDM74	*h$^-$ myo2-E1 ade6-216 leu1-32 ura4-D18 his3-D1*	Table 2; Balasubramanian *et al.*, 1998
JD141	*h$^-$ imp2::ura4$^+$ ade6-M216 leu1-32 ura4-D18*	Table 2; Demeter and Sazer, 1998
JW6057	*h$^-$ rng10Δ::hphMX6 ade6-210 leu1-32 ura4-D18*	Table 2
JW6623	*h$^+$ rga7Δ::natMX6 ade6 leu1-32 ura4-D18*	Table 2

Supplemental References

Balasubramanian MK, McCollum D, Chang L, Wong KC, Naqvi NI, He X, Sazer S, and Gould KL (1998). Isolation and characterization of new fission yeast cytokinesis mutants. Genetics 149, 1265-1275.

Cortes JC, Carnero E, Ishiguro J, Sanchez Y, Duran A, and Ribas JC (2005). The novel fission yeast (1,3)β-D-glucan synthase catalytic subunit Bgs4p is essential during both cytokinesis and polarized growth. J Cell Sci 118, 157-174.

Cortes JC, Sato M, Munoz J, Moreno MB, Clemente-Ramos JA, Ramos M, Okada H, Osumi M, Duran A, and Ribas JC (2012). Fission yeast Ags1 confers the essential septum strength needed for safe gradual cell abscission. J Cell Biol 198, 637-656.

Demeter J, and Sazer S (1998). *imp2*, a new component of the actin ring in the fission yeast *Schizosaccharomyces pombe*. J Cell Biol 143, 415-427.

Kim DU, Hayles J, Kim D, Wood V, Park HO, Won M, Yoo HS, Duhig T, Nam M, Palmer G, Han S, Jeffery L, Baek ST, Lee H, Shim YS, Lee M, Kim L, Heo KS, Noh EJ, Lee AR, Jang YJ, Chung KS, Choi SJ, Park JY, Park Y, Kim HM, Park SK, Park HJ, Kang EJ, Kim HB, Kang HS, Park HM, Kim K, Song K, Song KB, Nurse P, and Hoe KL (2010). Analysis of a genome-wide set of gene deletions in the fission yeast *Schizosaccharomyces pombe*. Nat Biotechnol 28, 617-623.

Viana RA, Pinar M, Soto T, Coll PM, Cansado J, and Pérez P (2013). Negative functional interaction between cell integrity MAPK pathway and Rho1 GTPase in fission yeast. Genetics 195, 421-432.

Wang H, Tang X, Liu J, Trautmann S, Balasundaram D, McCollum D, and Balasubramanian MK (2002). The multiprotein exocyst complex is essential for cell separation in *Schizosaccharomyces pombe*. Mol Biol Cell 13, 515-529.

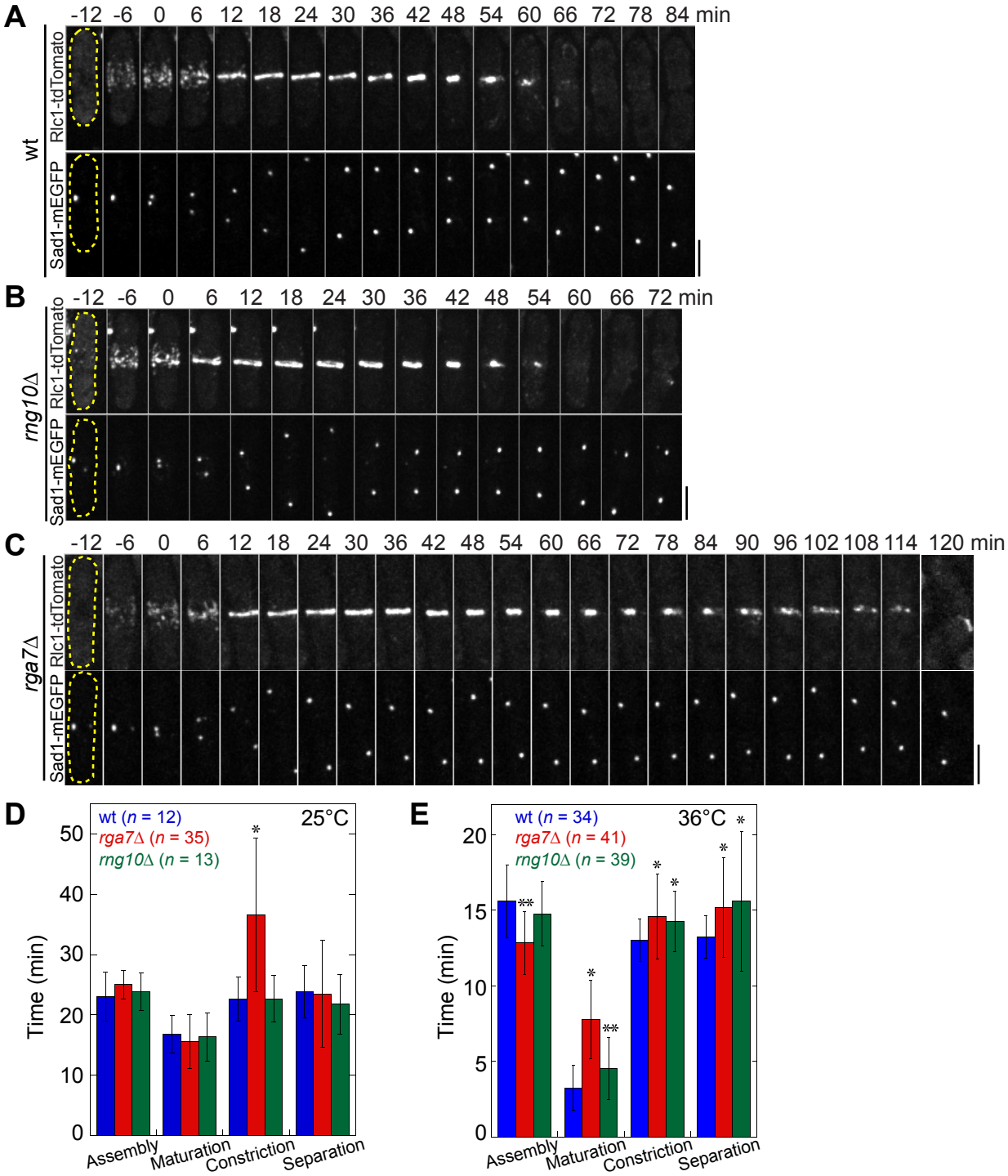

Supplemental Figure 1. Timing of the contractile ring and cell separation in wt, *rng10*Δ, and *rga7*Δ cells. (A-C) Time courses (in min) of Rlc1 localization at the division site in wt (A), *rng10*Δ (B), and *rga7*Δ cells (C) with Sad1 as a cell-cycle marker at 25°C. SPB separation is defined as time 0. The broken lines at -12 min mark the cell boundary. (D, E) Quantification of time for ring assembly (appearance of nodes to a compact ring without lagging nodes), maturation (a compact ring to just before ring constriction), constriction (ring diameter starts to decrease to ring constricts to a dot with peak Rlc1 intensity), and cell separation (the end of ring constriction to cell separation) at 25°C (D) and 36°C (E). *$p < 0.01$ and **$p < 0.001$ compared with wt. Bars, 5 µm.

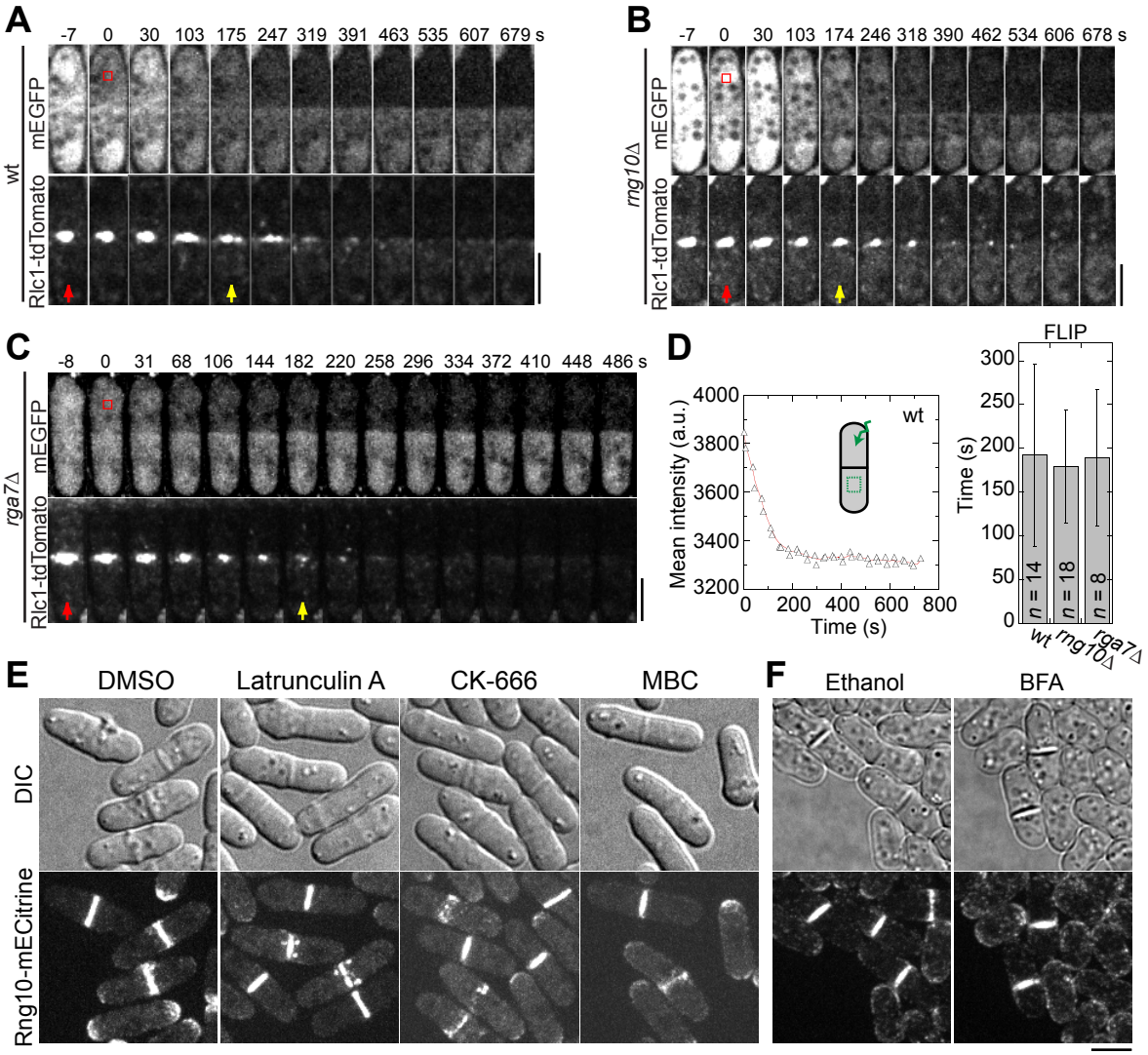

Supplemental Figure 2. *rng10*Δ and *rga7*Δ cells have no defects in plasma-membrane closure during cytokinesis and Rng10 localization is independent of F-actin, microtubules, or vesicle trafficking. (A-D) Micrographs (A-C) and quantification (D) of FLIP assays in wt (A), *rng10*Δ (B), and *rga7*Δ (C). Cells expressing mEGFP from the *leu1* locus under the *3nmt1* promoter were grown in YE5S medium at 25°C for 40 h before FLIP. Red box marks the bleached site. Red arrows indicate the end of contractile-ring constriction when Rlc1 reaches peak intensity at the center of the division site. Yellow arrows indicate mEGFP exchange between two daughter cells stopped. (D) Quantification of time from the end of ring constriction to membrane closure in wt, *rng10*Δ (p = 0.67 compared with wt), and *rga7*Δ (p = 0.67). An example curve of fluorescence intensity in one unbleached wt daughter cell is shown on the left. The green square marks the ROI measured to generate the curve. (E, F) Micrographs of cells expressing Rng10-mECitrine treated with different drugs or their solvents. Bars, 5 µm.

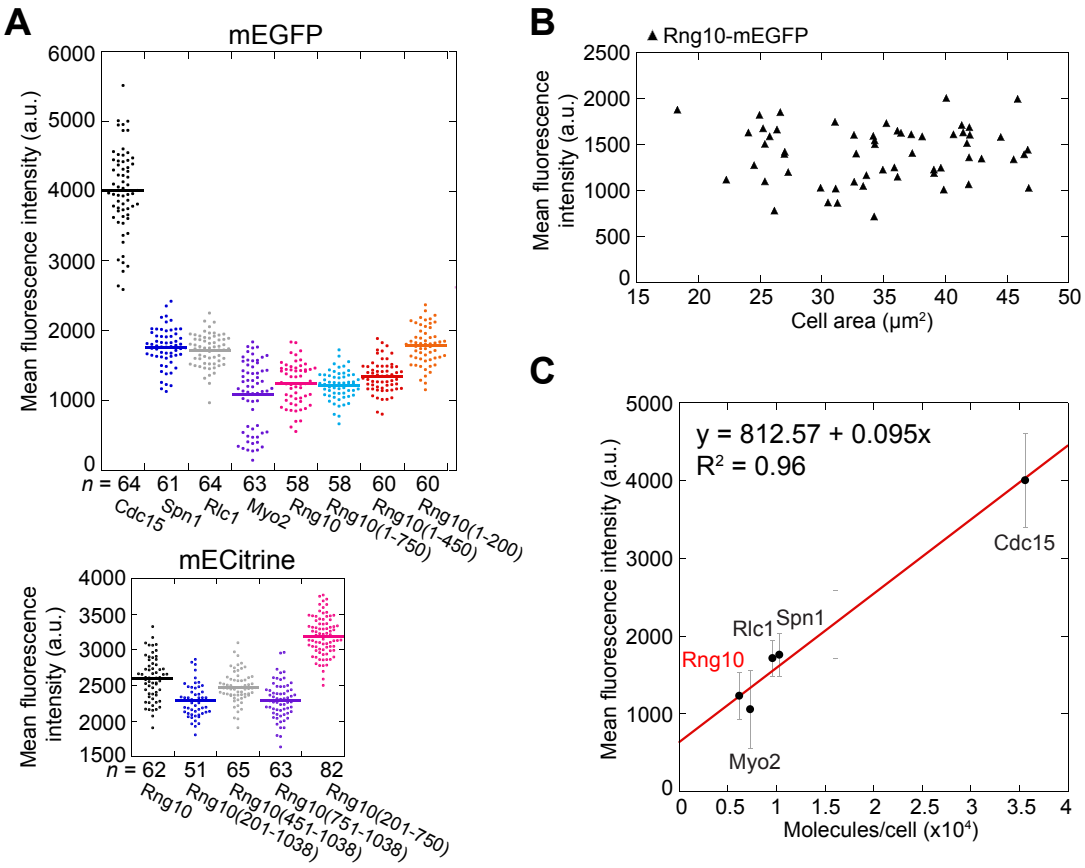

Supplemental Figure 3. Counting Rng10 protein molecules by quantitative fluorescence microscopy. (A) Plots of mean fluorescence intensity per cell for mEGFP (top) and mECitrine (bottom) tagged proteins in molecule counting. (B) The mean intensity of individual cells expressing Rng10-mEGFP plotted in (A) versus their cell area along the long axis. (C) Standard curve for mean fluorescence intensity vs. published molecule numbers (Wu and Pollard, 2005). Rng10 is plotted on the standard curve for comparison.

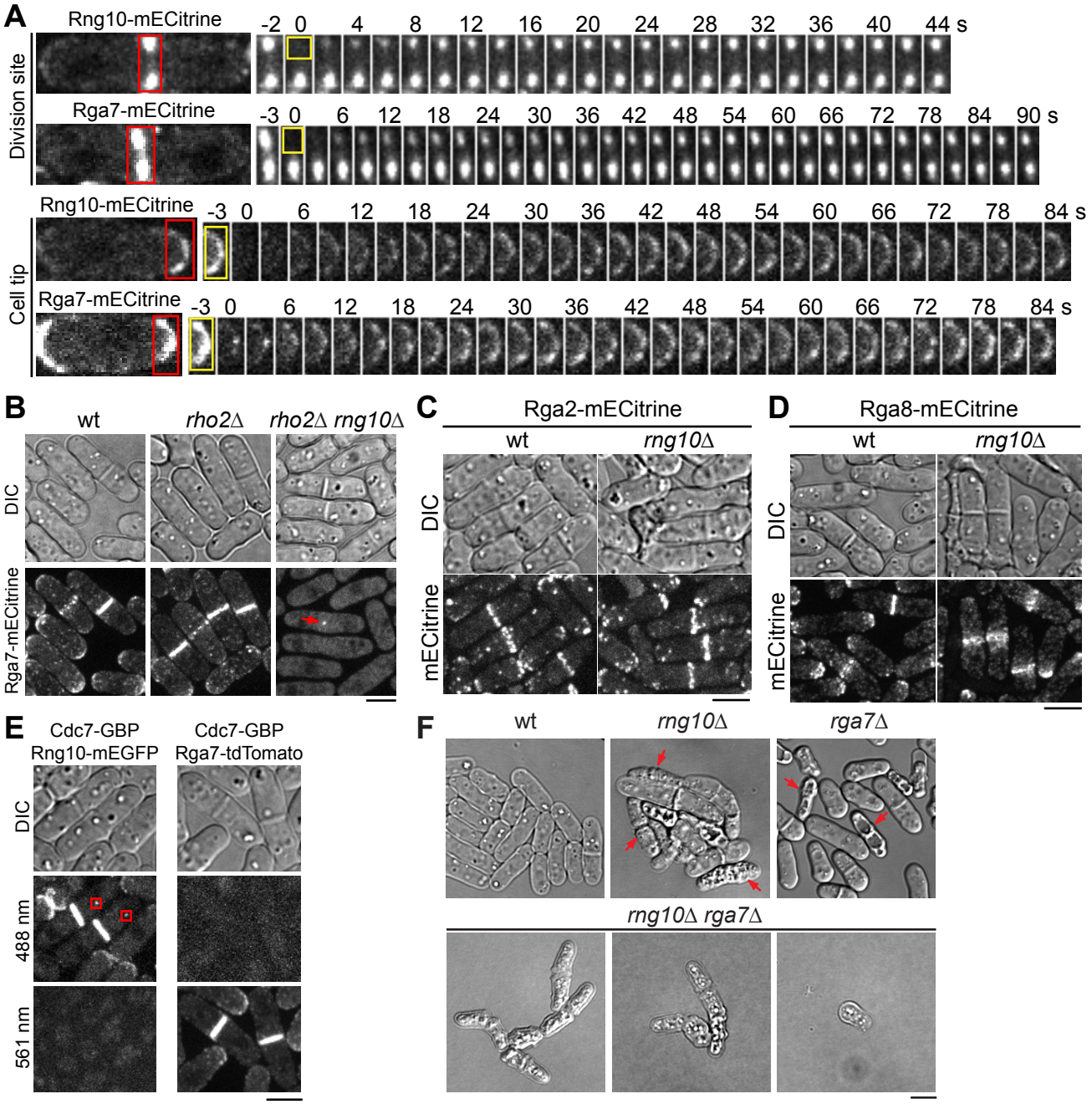

Supplemental Figure 4. FRAP analyses of Rng10 and Rga7; Rga7, Rga2, and Rga8 localization in mutants; controls for mislocalization experiments using GBP; and *rng10*Δ and *rga7*Δ genetic interaction. (A) FRAP analyses at the division site (top) or the cell tip (bottom). Time-lapse images show recovery of signals over time. Red box marks the region shown on the right. Yellow box marks the region photobleached at time 0. (B) Rho2 is not required for Rga7 localization. The arrow indicates the Rga7 dot remains at the division site in *rho2*Δ *rng10*Δ cells. (C, D) Rga2 (C) and Rga8 (D) localization in wt and *rng10*Δ cells. (E) Controls for mislocalization experiments using Cdc7-GBP. Cdc7-GBP recruits proteins tagged with mEGFP but not tdTomato to SPBs and lack of signal bleedthrough between 488- and 561-nm channels. Cells were imaged under three channels: DIC for cell morphology, 488 nm for mEGFP, and 561 nm for tdTomato. Red boxes in E mark mislocalized proteins on SPBs by Cdc7-GBP. (F) *rng10*Δ and *rga7*Δ are synthetic lethal at 25°C. Arrows mark some of the lysed cells. Bars, 5 μm.

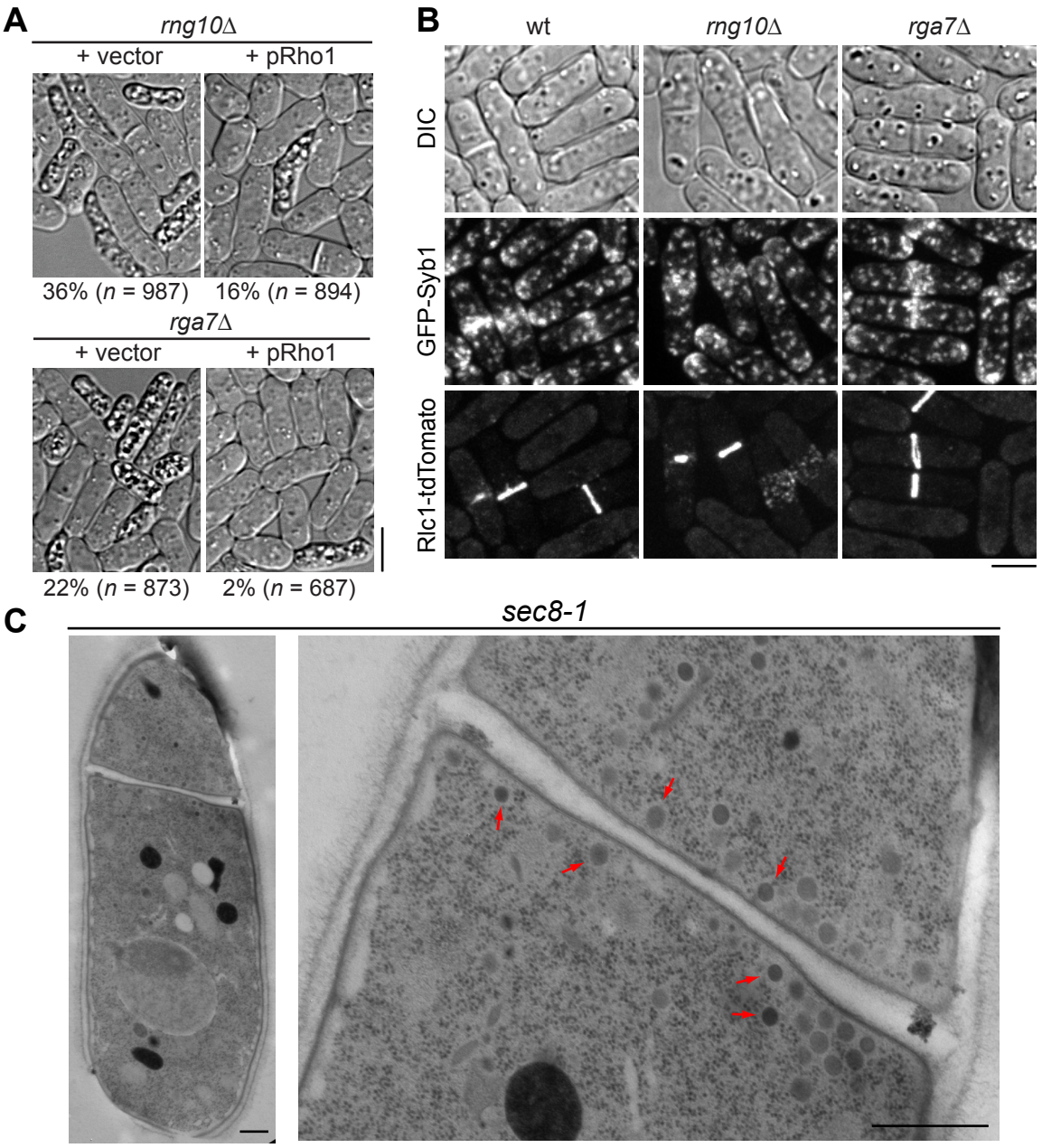

Supplemental Figure 5. Rescue of *rng10*Δ and *rga7*Δ by Rho1 overexpression; localization of v-SNARE Syb1 in *rng10*Δ and *rga7*Δ cells; and accumulation of secretory vesicles in *sec8-1* mutant. (A) Rho1 overexpression rescues cell lysis in *rng10*Δ and *rga7*Δ. Cells were grown at 36°C for 4 h. Numbers below the graphs indicate percentages of cell lysis. (B) Localization of Syb1 in wt, *rng10*Δ, and *rga7*Δ cells with Rlc1 labeled contractile ring. (C) EM images of *sec8-1* cells grown at 36°C for ~4 h. Red arrows indicate secretory vesicles. Bars, 5 μm in A and B, and 0.5 μm in C.